Chapter 18
Land Surface Phenology Monitoring with SeaWinds Scatterometer Time Series in Eastern Asia

Linlin Lu, Huadong Guo, and Cuizhen Wang

Abstract Vegetation phenology tracks plants' lifecycle events and reveals the response of vegetation to global climate change. Microwave backscatter is insensitive to signal degradation from solar illumination and atmospheric effects and thus provides a useful tool for phenology monitoring. In this chapter, we analyzed a time series of Ku-band radar backscatter measurements from the SeaWinds scatterometer on board the Quick Scatterometer (QuickSCAT) to examine its effectiveness for land surface phenology monitoring across eastern Asia. The spatial pattern of annual mean backscatter follows regional vegetation type distributions. The Start Of Season (SOS) and End Of Season (EOS) were derived from the backscatter time series and compared with MODIS (Moderate Resolution Imaging Spectroradiometer) phenology products from 2003 to 2007. The failure of phenology metric detection for backscatter time series is caused by snow coverage and limited vegetation activity in arid areas. For tropical and semi-arid areas where optical observation is unavailable, backscatter data can provide valid phenological information. Due to their sensitivity to different factors, temporal discrepancies were observed between phenology products from backscatter and MODIS time series. Overall, the results indicate that SeaWinds backscatter provides an alternative view of vegetation phenology that is independent of optical sensors and can be applied to global phenology studies.

L. Lu (✉) • H. Guo
Key Laboratory of Digital Earth Sciences, Institute of Remote Sensing and Digital Earth, RADI, Chinese Academy of Sciences, CAS, Beijing, China
e-mail: lull@radi.ac.cn

C. Wang
Department of Geography, University of South Carolina, Columbia, SC, USA

C. Kuenzer et al. (eds.), *Remote Sensing Time Series*, Remote Sensing and Digital Image Processing, DOI 10.1007/978-3-319-15967-6_18

18.1 Introduction

Vegetation phenology tracks plants' lifecycle events such as bud break, flowering, and leaf senescence as the cumulative effects of daily weather at different developmental stages (Lieth 1974). Over the past century, phenological shifts have been observed in association with warming climate across a diverse range of plant taxonomy (IPCC 2007; Richardson et al. 2013). Land Surface Phenology (LSP) may be defined as seasonal patterns of variation in vegetated land surfaces observed from remote sensing (de Beurs and Henebry 2004). Critical phenological dates or metrics, such as the onset of greening, onset of senescence, timing of the maximum of the growing season and growing season length can be derived from time series of remote sensing data. These metrics are sensitive to the timing and duration of vegetation activity, which significantly affect fluxes of carbon, water, energy, and other trace gases and therefore are important to biosphere–atmosphere interactions (Morisette et al. 2009).

Satellite data at optical-infrared wavelengths from operational satellite sensors such as AVHRR (Advanced Very High Resolution Radiometer), MODIS (Moderate Resolution Imaging Spectroradiometer) and SPOT-VGT (Satellite Pour l'Observation de la Terre-Vegetation) and derived spectral vegetation indices (VI) have been widely used to LSP monitoring at spatial resolutions of 500–8,000 m (Ganguly et al. 2010). Cloud contamination and soil background in sparsely vegetated areas, however, often cast high uncertainties on these phenology products. Satellite microwave remote sensing records data at lower frequency wavelengths which are sensitive to changes of water content, canopy structure and biomass (Ulaby et al. 1982), and provides a useful alternative for phenology assessment. Microwave backscatter is insensitive to signal degradation from solar illumination and atmospheric effects. The wind scatterometer on ERS-l was compared with global VI data for monitoring vegetation dynamics (Wagner et al. 1999) and examining the seasonal vegetation development (Frison and Mougin 1996). The potential of passive and active microwave measurements in vegetation monitoring was jointly investigated at the global scale with the special sensor microwave/imager (SSM/I) and ERS scatterometer (Macelloni et al. 2003). Several microwave Vis (MVIs) have been retrieved from daily time-series brightness temperature of passive microwave radiometers. Comparing with NDVI (Normalized Difference Vegetation Index), the results proved that MVIs could provide significant new information of vegetation development (Min and Lin 2006; Shi et al. 2008).

Though its primary mission is to observe ocean winds, the SeaWinds on Quick Scatterometer (QuickSCAT) provides an opportunity for an active microwave scatterometer to assess phenological features associated with seasonal changes of vegetated landscapes. Hardin and Jackson (2003) modeled the monthly composites of SeaWinds Ku-band backscatter as a function of savanna grass biomass and leaf area, soil moisture, and other soil characteristics in South America, finding it promising in monitoring the dynamics of savanna grasslands. In boreal and subalpine evergreen coniferous forests, Kimball et al. (2004) employed a temporal change classification to detect the initiation and termination of the growing season from daily radar backscatter measurements from the SeaWinds scatterometer.

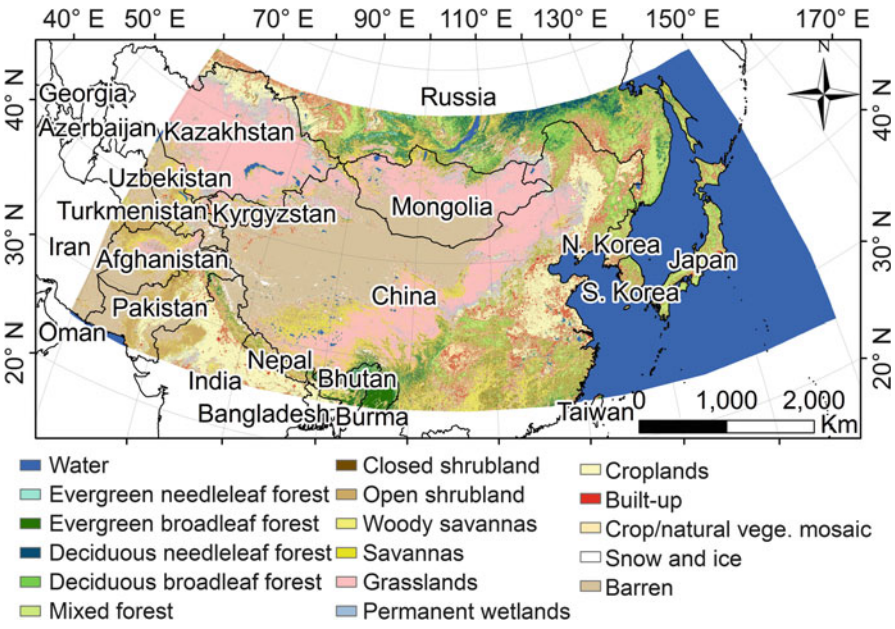

Fig. 18.1 Land cover types in eastern Asia

Frolking et al. (2005, 2006) found that the SeaWinds Ku-band backscatter and MODIS leaf area index (LAI) were strongly correlated in North American grasslands in the growing season, and backscatter was sensitive to seasonal variability in grassland biomass and productivity. Lu et al. (2013a) applied a three-year backscatter time series to vegetation phenology monitoring from 2003 to 2005 across China. Eastern Asia is a large region encompassing a wide range of climate and land cover types (Fig. 18.1). In this study, we extended the study by Lu et al. (2013a) and evaluated the effectiveness of SeaWinds Ku-band backscatter in vegetation phenology monitoring across eastern Asia. The spatial pattern and variability of backscatter was mapped and analyzed from 2000 to 2009. The phenology detection results from a 5-year backscatter time series were compared with the MODIS phenology products at regional level.

18.2 Data and Methods

18.2.1 SeaWinds Backscatter Data

Launched in June 19, 1999, SeaWinds scatterometer on-board the QuickSCAT satellite was originally intended to be a 'quick recovery' mission to fill the gap created by the unexpected failure of the NASA scatterometer (NSCAT) (King and

Greenstone 1999). The SeaWinds instrument consists of a rotating pencil-beam antenna, which provides contiguous measurement swaths of 1,400 km (inner-beam) and 1,800 km (outer-beam), coverage of approximately 70 % of Earth on a daily basis and 90 % global coverage every 2 days. The SeaWinds radar transmits microwave radiation at a 13.4 GHz (2.1 cm) wavelength and receives a surface backscatter signal with a 0.25 dB relative accuracy (King and Greenstone 1999). It records radar backscatter with dual polarization (vertical and horizontal) at two nominal incidence angles, 46.0° and 54.1° corresponding to the inner and outer beams. The inner beam has horizontal polarization while the outer beam has vertical polarization. The data records span from July 1999 to November 2009, and the standard processing of backscatter measurements yields a spatial resolution of about 25 km.

The Scatterometer Image Reconstruction (SIR) technique is applied to the overlapping passes to reduce noises for enhanced resolution measurements of the surface characteristics (Early and Long 1996). Since the SeaWinds outer beam data provide improved temporal coverage and an increased propagation path through vegetation volume (Frolking et al. 2006), this study applied the composite 4 day V-pol average backscatter time series of the SeaWinds L2A product at 4.5 km resolution (Early and Long 2001). SeaWinds backscatter data from January 2000 to November 2009 covering eastern Asia were downloaded from the NASA Scatterometer Climate Record Pathfinder database at Brigham Young University (http://www.scp.byu.edu) (Fig. 18.1). The Marine Geospatial Ecology Tools (MGET) were used to convert SIR files to raster format (Roberts et al. 2010).

18.2.2 MODIS Phenology and Land Cover Products

The V005 MODIS Land Cover Dynamics (MCD12Q2) product (informally called the MODIS Global Vegetation Phenology product) provides estimates of the timing of vegetation phenology at global scales (Ganguly et al. 2010). MCD12Q2 primarily uses the MODIS Enhanced Vegetation Index (EVI), which is computed from the MODIS Nadir Bidirectional Reflectance Distribution Function (BRDF)-Adjusted Reflectance (MODIS NBAR) product. The snow and ice flag included in the MODIS NBAR product is used to filter out data points associated with snow-covered surfaces from the input time series. In particular, a time series of EVI is extracted for each pixel. Periods of sustained EVI increase or decrease are identified after a gap-filling and smoothing process. Logistic models are fit to the time series and transition dates including the onset of EVI increase, the onset of EVI maximum, the onset of EVI decrease, and the onset of EVI minimum are identified as local maxima and minima in the rate of change of curvature of the fitted logistic function (Ganguly et al. 2010). In our study, the onset of EVI increase and onset of EVI decrease dates from 2003 to 2007 covering the study area are retrieved for the comparative analysis.

The MODIS 1 km land-cover product (MOD12Q1) was used to identify primary land covers in the study area. With the International Geosphere-Biosphere Programme (IGBP) land-cover legend (Friedl et al. 2002), the MODIS product of 2009 was downloaded and a total of 18 cover types were mapped and served as base information in this study (Fig. 18.1).

The MODIS Re-projection Tool was used to mosaic and convert Hierarchical Data Format (HDF) files to raster format. They were re-projected and resampled to the same resolution as the SeaWinds backscatter products at a local radius equal-area Lambert Projection.

18.2.3 Climate Data

In radar backscatter data, dielectric constants of land surfaces are strongly affected by frozen and thaw conditions. To differentiate data in the frozen and nonfrozen seasons and assign them different weights in the phenology model from the annual time series, a temperature mask was generated using temperature data. The daily air temperature grid data in a 2.5° spatial resolution was downloaded from the NCEP Daily Global Analyses data provided by the NOAA/OAR/ESRL PSD, Boulder, Colorado, USA, from their Web site at (http://www.esrl.noaa.gov/psd) (Trenberth and Olson 1988a, b). The onset of the fully thawed season was determined to be the last day of 6 consecutive days with mean air temperatures greater than 5 °C, and the end of the thaw season as the first day of 6 consecutive days with mean air temperature less than 50C (Karl et al. 1999; Peterson 2005). Gridded temperature masks defining the start and end of the thaw season were produced for each year. They were re-projected and spatially disaggregated to the same grid as the SeaWinds data.

18.2.4 Means and Variability of Backscatter

In this study, the backscatter data was used to calculate derivative datasets on annual basis, a common process for analyses of time series (Gessner et al. 2013; Kuenzer et al. 2009). The mean monthly backscatter was calculated from the monthly data based on the 2000–2009 time series. For a given pixel, the monthly 10-year arithmetic mean ($\overline{\text{Backscatter}}_{x,y}$) was calculated using Eq. (18.1), with n being the number of years and $\text{Backscatter}_{x,y}$ the monthly backscatter value for pixel x, y. The mean annual backscatter was calculated accordingly from the annual sums.

$$\overline{\text{Backscatter}}_{x,y} = \frac{1}{n}\sum_{1}^{n}\text{Backscatter}_{x,y} \tag{18.1}$$

The deviation ($DevB_{x,\ y}$) from the 2000–2009 mean annual backscatter at a given spatial location for a certain year was calculated according to Eq. (18.2).

$$DevB_{x,y} = Backscatter_{x,y} - \overline{Backscatter}_{x,y} \tag{18.2}$$

In addition, the relative annual backscatter deviation ($rDevB_{x,\ y}$) was derived. This describes the deviation as a percentage from the mean annual backscatter, as given by Eq. (18.3).

$$rDevB_{x,y} = \frac{DevB_{x,y} \cdot 100}{\overline{Backscatter}_{x,y}} \tag{18.3}$$

The mean annual variability ($\overline{VB}_{x,y}$) was derived according to Eq. (18.4) with the relative annual backscatter deviation ($rDevB_{x,\ y}$) and n being the number of years.

$$\overline{VB}_{x,y} = \frac{1}{n}\sum_{1}^{n}\left|rDevB_{x,y}\right| \tag{18.4}$$

18.2.5 Phenology Metric Detection

According to Frolking et al. (2006) and Lu et al.(2013a), radar backscatter has a significant relationship with LAI based on site-level linear regression analysis. Therefore, a weighted phenological model was applied to the backscatter time series to detect the timing of leaf flush and senescence in this study. The curve-fitting method, Asymmetric Gaussian implemented in the TIMESAT software is a common tool for time series analysis (Gao et al. 2008; Wang et al. 2011; Jones et al. 2012). It was applied to fit local model functions to the backscatter data of a vegetation growth cycle. The single growth cycle of vegetation typically consists of a growth and senescence phase. The Gaussian type of function was used as the following (Jönsson and Eklundh 2002, 2004):

$$f(t; x_1, x_2, \ldots x_5) = \left\{ \begin{array}{ll} e^{-\left(\frac{t-x_1}{x_2}\right)^{x_3}} & if\ t > x_1 \\ e^{-\left(\frac{x_1-t}{x_4}\right)^{x_5}} & if\ t < x_1 \end{array} \right\} \tag{18.5}$$

In this model, the coefficient x_1 determines the position of the maximum or minimum with respect to the independent time variable t. Coefficients x_2 and x_3 determine the width and flatness of the right half of the function, while x_4 and x_5 determine the width and flatness of the left half. In order to ensure smooth shapes of the model functions and consistency with data observations, these coefficients were restricted in certain conditions and were calculated using a separable Levenberg–Marquardt method (Madsen et al. 2004).

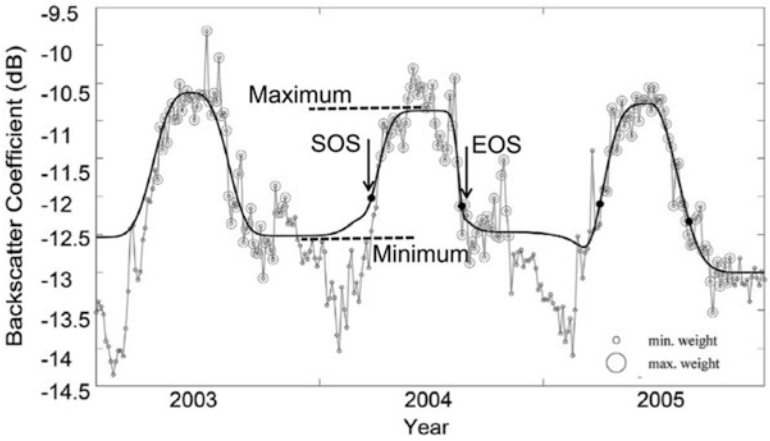

Fig. 18.2 An example of the 3-year SeaWinds backscatter times series and its curve-fitting results

With the asymmetric Gaussian fitting model, two seasonality metrics, namely the Start Of Season (SOS) and the End Of Season (EOS), were calculated. Assuming the seasonal amplitude as the difference between the maximum value and base level, the SOS was defined as the time when the left edge increased to 30 % of the seasonal amplitude measured from the left minimum level, and the EOS was defined as the time when the right edge has decreased to 30 % of the seasonal amplitude from the right minimum level (Jönsson and Eklundh 2004). The phenology detection of backscatter time series at a sample site is shown in Fig. 18.2. The sample site is a homogenous area (3×3 pixels) with main land cover as deciduous forest. The backscatter time series from 2003 to 2005 was weighted and fitted with the asymmetric Gaussian model. With this model, phenological metrics (SOS and EOS) of all pixels were extracted from the backscatter time series to examine their spatial patterns across the eastern Asia.

18.3 Results

18.3.1 Backscatter Mean and Variability

Figure 18.3 represents the spatial variation of the annual mean backscatter across eastern Asia for the 2000–2009 period. Comparing with the land cover type (Fig. 18.1), the spatial pattern of backscatter follows regional vegetation type distributions. For grasslands and barren lands with sparse vegetation in Kazakhstan, Mongolia, and northwestern China the backscatter value ranges from -20 to -15 dB. For areas dominated by forests in the south of China, it ranges from -15 to -11 dB. Agricultural lands in northern China exhibited medium backscatter

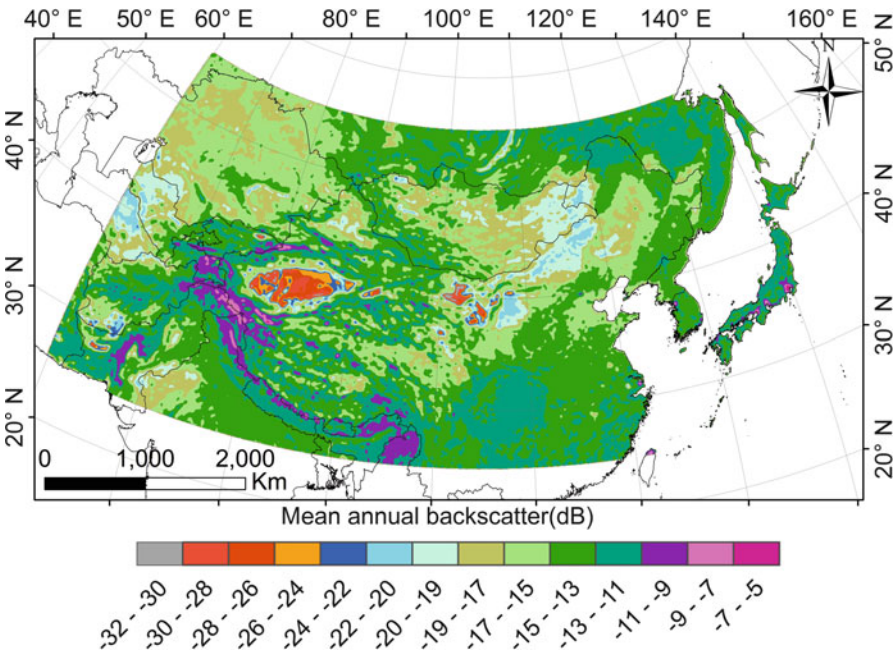

Fig. 18.3 Mean annual backscatter for the 2000–2009 period across eastern Asia

from −17 to −15 dB, whereas it shows higher value (−15 to −13 dB) in India and southern China. The desert in western China shows extremely low value (−30 to −26 dB). The mountain areas in the south western China are often covered with snow and show highest values (−11 to −5 dB).

The Fig. 18.4 illustrates how the mean annual backscatter varies from year to year for the 2000−2009 period. Areas with high variability show less stable backscatter values than areas with low variability. In general, the mean annual backscatter variability reveals moderate dynamic levels over the land surface (<10 %, and mostly <5 % in Fig. 18.4). The northern area of the study region shows higher variability than the southern. High variability can be observed in northeastern China. Similar variability was detected in the arid areas of Kazakhstan and the desert area of India. Fluctuation of backscatter is also observable for the Tibetan Plateau.

18.3.2 Regional Comparison of Backscatter- and MODIS-Derived Phenology Metrics

In order to reduce the uncertainties in phenological detection results, we used detected phenology dates from 2003 to 2007 for the comparative analysis. The

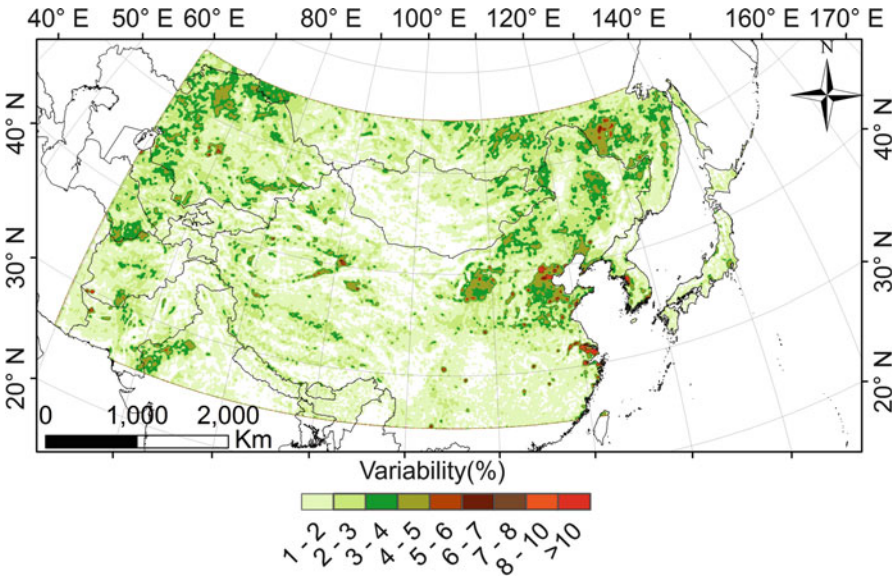

Fig. 18.4 Mean annual backscatter variability (%) for 2000−2009 across eastern Asia

numbers of successful annual retrievals for phenological metrics from backscatter and MODIS data are shown in Fig. 18.5. For backscatter data, missing values were distributed mostly in high latitude areas and the Tibetan Plateau. The failure of detection in MODIS data was distributed in the southern tropical and subtropical area, the arid and semiarid area in northwestern China and Sichuan province in southern China. For the multiple-cropping areas in eastern China, the phenological metrics can be detected from MODIS time series in only 3 or 4 years.

The mean SOS dates derived from backscatter time series and MODIS products for 2003–2007 are shown in Fig. 18.6a, b. The SOS dates ranged widely from approximately DOY 70 in the south to DOY 190 in the north. The grasslands extending from Kazakhstan to Mongolia (Fig. 18.1) showed an earlier SOS than areas at the same latitude. It shows a gradient from east to west, with southeastern Mongolia having a much later SOS from both datasets. Other areas with much later SOS from backscatter time series are northern China and northern India. The northern China is dominated by grassland and agriculture lands. The northern India is dominated by vast irrigated drylands and has a tropical desert climate.

Figure 18.7 shows the bias between backscatter SOS and MODIS greenup dates. For the agricultural lands in central China (Fig. 18.1), the backscatter data shows later greenup dates than MODIS data. For grasslands in the north, the backscatter data detects earlier SOS dates. In the south of China where there are mixed land covers of forest, shrub lands and croplands with a dominant subtropical and tropical monsoon climate, the backscatter data also detects earlier SOS.

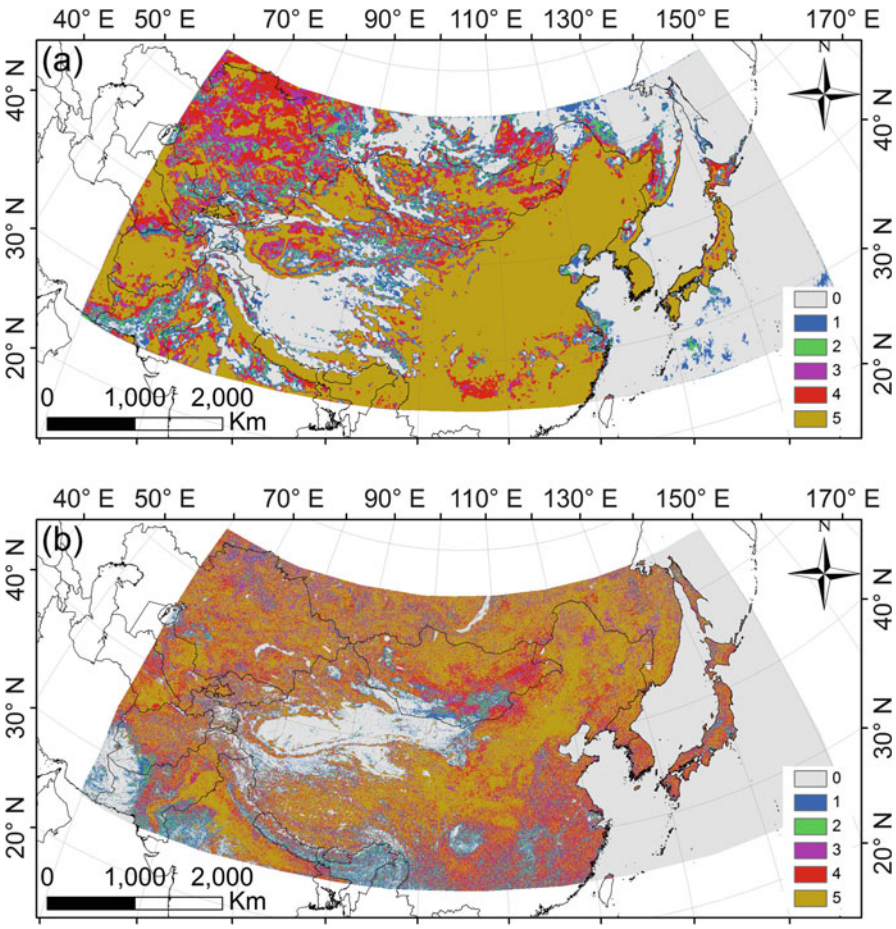

Fig. 18.5 Number of successful annual retrievals for phenology metrics derived from (**a**) backscatter time series and (**b**) MODIS phenology products at pixel level for 2003–2007 in eastern Asia

The end of season derived from backscatter time series and MODIS senescence date for 2003–2007 are shown in Fig. 18.8. The MODIS EOS dates range from DOY 100 to DOY 280, and backscatter EOS range from DOY 100 to DOY 360. Though the EOS detected by backscatter data is later than MODIS, it shows a clear spatial pattern from north to south regionally. A similar earlier EOS was detected in Kazakhstan from both backscatter and MODIS datasets. The EOS gradient detected by backscatter data across China shows an earlier growing season end in the north.

Figure 18.9 shows the bias between backscatter EOS and MODIS senescence dates. For most areas, the backscatter data detected later EOS dates. In the grasslands in Kazakhstan, Mongolia and China, the EOS detected by MODIS occurs later than that derived from backscatter. Another discrepancy occurred in the agricultural lands in central China and northern India.

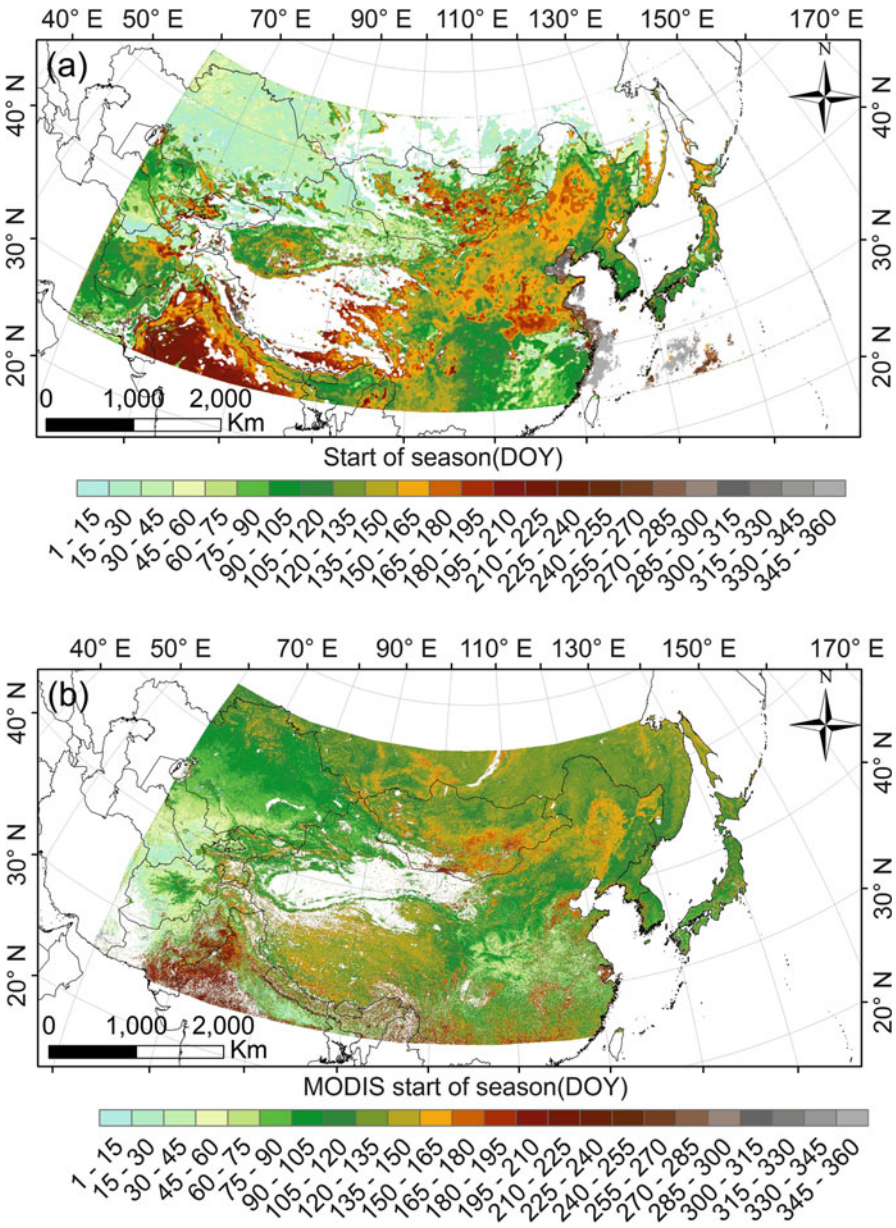

Fig. 18.6 The mean start of season derived from (**a**) backscatter time series for 2003–2007 and (**b**) MODIS greenup date for 2003–2007 in eastern Asia

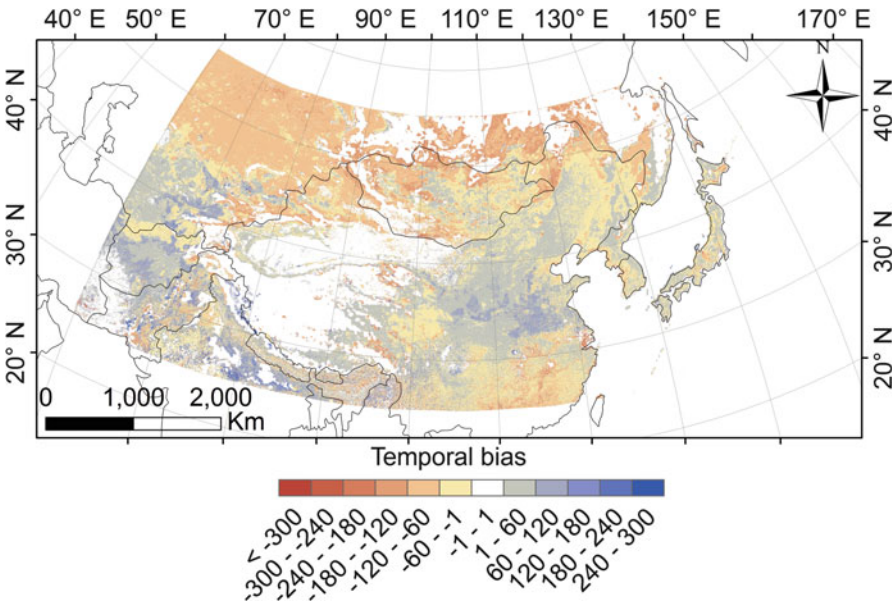

Fig. 18.7 The temporal bias between mean backscatter SOS and MODIS greenup date 2003–2007 in eastern Asia

18.4 Discussion

The spatial patterns of backscatter and derived phenological metrics as reported in this study reflect the controlling mechanisms of vegetation activity including both broad-scale patterns related to climate and local factors related to land cover and human activities. The backscatter and its variability (Figs. 18.3 and 18.4) reveal a clear spatial variation across the eastern Asia region. The inter-annual variability of backscatter in different areas might be attributed to different reasons. As reported by Frolking et al. (2011), severe drought occurred in southwestern Amazonia can be detected from the significant interannual variability in dry season monthly mean backscatter. The variability in the arid area of Kazakhstan and the desert area of India might be caused by variation of soil moisture that is strongly impacted by precipitation. The fluctuation of snow coverage can cause backscatter variability in the north of China and the Tibetan Plateau. Anthropogenic activities such as cultivation and urban expansion can lead to the high variation in China northern plain. With MODIS data, Zhang et al. (2006) studied global vegetation phenology and found that the timing of crop phenology can be quite variable, depending strongly on crop type and agricultural management. Frolking et al. (2013) reported that the significant backscatter increase of SeaWinds backscatter in major cities around the world was caused by changes of built-up infrastructure.

The numbers of successful annual retrievals for phenological metrics from time series (Fig. 18.5) reveal the algorithm sensitivity to data noise and gaps. For

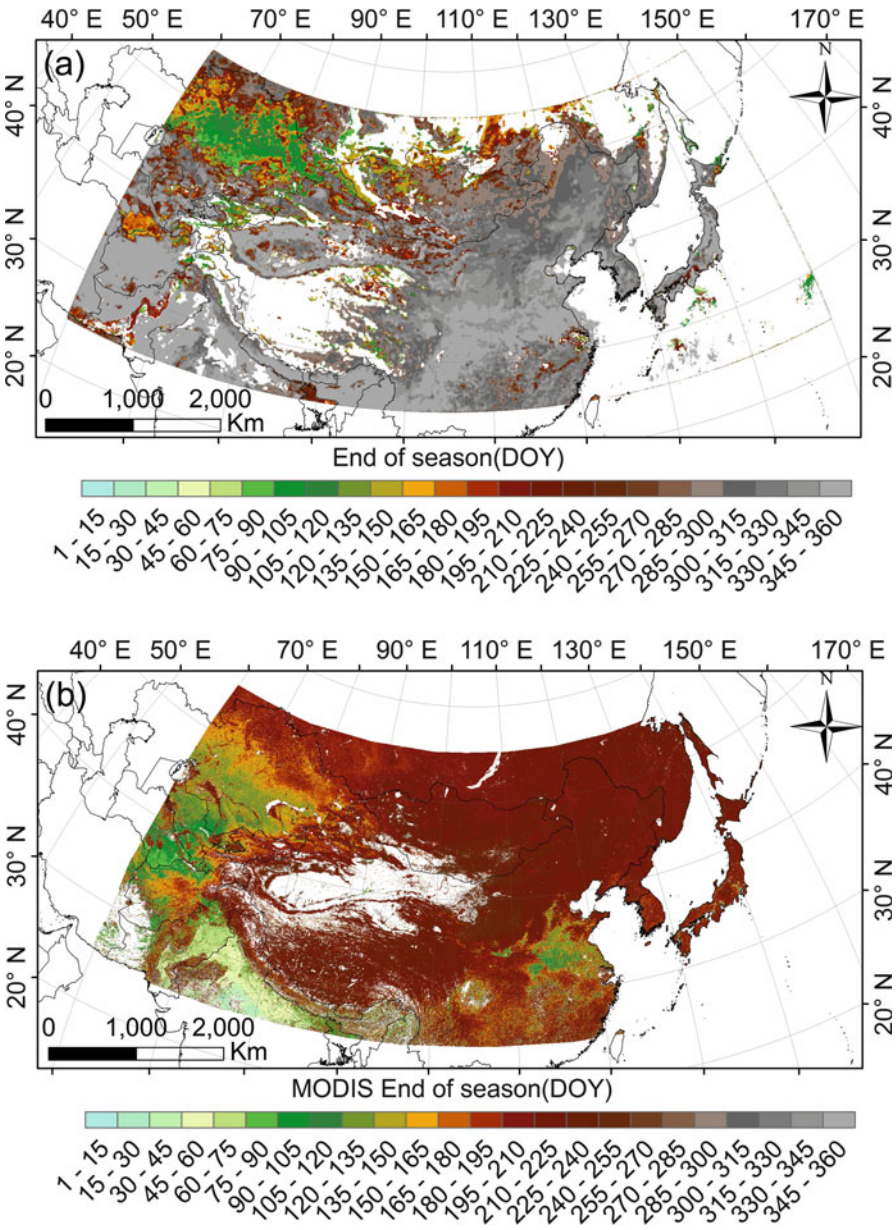

Fig. 18.8 The mean end of season derived from (**a**) backscatter time series for 2003–2007 and (**b**) MODIS senescence date for 2003–2007 in eastern Asia

SeaWinds backscatter time series, snow in the high latitude area and the Tibetan Plateau results in the failure of phenology detection algorithms (Fig. 18.5a). For MODIS phenology products, the persistent cloud cover, high levels of atmospheric

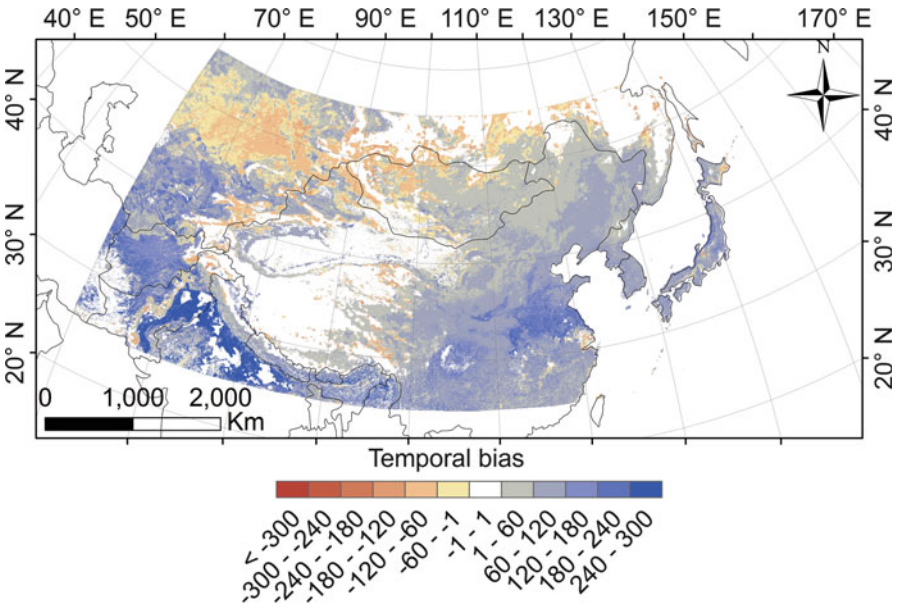

Fig. 18.9 The temporal bias between backscatter EOS and MODIS senescence date for 2003–2007 in eastern Asia

aerosols and weak seasonality present substantial challenges for land surface phenology algorithms (Ganguly et al. 2010). Missing values are observable in tropical and subtropical area (Fig. 18.5b). In arid and semiarid area of China, phenology detection failures are caused by the limited vegetation activities. In the multiple-cropping areas in eastern China, multiple vegetation growth cycles exit in 1 year, which can also cause the failure of phenology detection. Only three or four phenology cycles have been successfully detected in MODIS product (Fig. 18.5b). In contrast, backscatter imagery provides effective phenological observations in these areas.

The regional patterns of SOS and EOS from backscatter and MODIS (Figs. 18.6 and 18.8) show similar latitudinal shifts, which are related to large-scale climate transitions. For example, the spatial variability of grassland phenology in Kazakhstan and Mongolia at the same latitude reflects the impacts of the precipitation regimes. Agreeing with Begue et al (2014) and Zhang et al (2005), the SOS shifts from MODIS phenological products are linked to the timing of seasonal rainfall in the arid and semi-arid lands.

The backscatter-derived phenology metrics show different temporal bias from MODIS products in different land cover types. The bias of backscatter SOS dates and MODIS greenup dates is caused by the temporal shifts between backscatter increase and canopy greenup. For boreal forests in Russia, an earlier SOS and EOS were detected prior to greenup and senescence onset respectively. Kimball et al. (2004) studied boreal and subalpine evergreen forests with SeaWinds

scatterometer, and revealed that radar remote sensing measurements of the initiation of the growing season corresponded strongly with both site measurements and ecosystem process model simulations. Jönsson et al. (2010) studied tree phenology with MODIS vegetation index, and revealed that without a sharp increase in greenness during spring, the seasonal changes in vegetation indices of evergreen trees were more related to snow dynamics than to changes in needle biomass. As seasonal thawing occurs, transpiration rates increase and water is allocated to canopy branches or existing leaves prior to new leaf construction (Waring et al. 1979). This may lead to backscatter seasonal increase and SOS prior to MODIS greenup date. For tropical and subtropical forests in southern China, an earlier greenup onset and later senescence onset were detected from backscatter data. The structural changes of the plants such as leaf fall and leaf flushing influence the seasonal variation of backscatter signals. In the steppes in Kazakhstan and Mongolia, the backscatter SOS and EOS generally precede the VI greenup. With low vegetation cover and biomass, the backscatter is more related to the fluctuation of soil moisture which is earlier than the increase of leaf greenness. In cropland-dominated areas, planting and harvest times drive the vegetation phenology cycles and the backscatter SOS generally follows NDVI greenup. Croplands are primarily barren or covered with non-photosynthetic residues prior to tilling and planting. Greenup occurs at seed germination or the initiation of visible above-ground photosynthetic vegetation growth, which can occur prior to significant biomass growth (Jones et al. 2011; Lu et al. 2014). The backscatter follows the initial VI greenup by several weeks or more following delayed increase in vegetation water content and development of above-ground biomass.

Despite these findings, there are significant limitations to our research. The data noise and gap in the time series may lead to large uncertainties of the phenology detection results. Different methods were used to detect phenological dates from backscatter and MODIS time series, which may cause their discrepancy (White et al. 2009). Moreover, time series of the eddy covariance measurements from tower sites can be integrated in further studies, which would improve understanding of our results (Jones et al. 2012; Melaas et al. 2013).

18.5 Conclusions

This study tested the feasibility and effectiveness of microwave backscatter data in regional vegetation phenology monitoring. The mean and variability of backscatter were derived from the SeaWinds Ku-band backscatter time series for the 2000–2009 period across eastern Asia. The vegetation phenology metrics (SOS and EOS) were extracted for the 2003–2007 period and compared with contemporary MODIS phenology products. The results can be summarized as follows.

The regional spatial patterns of annual mean backscatter in eastern Asia follow the spatial distributions of vegetation types. The mean annual variability observed in SeaWinds backscatter can be related to the dynamics of meteorological

conditions such as drought and snowfall. Human activities, for example the intensified agricultural practices and expanded urban developments, also lead to its high variability.

In areas where optical time series is unavailable due to persistent cloud cover, high levels of atmospheric aerosols and low VI values, backscatter imagery provides effective observations. Different temporal biases were found in different land cover areas between the backscatter-extracted and the published MODIS phenology metrics. For boreal forests and steppes, the backscatter-extracted SOS and EOS preceded the MODIS greenup and senescence onsets, respectively. For tropical and subtropical forests, an earlier SOS and later EOS dates were detected with the backscatter data, while the SOS for croplands was found later than the MODIS greenup.

Overall, the application of backscatter time series for LSP monitoring can expand the breadth of the current optical satellites, thereby enhance our understanding of global vegetation dynamics and carbon cycle processes. However, given the complexity of Ku-band backscatter behaviors on vegetated landscapes, a critical challenge of our study is to understand the bio-ecological meaning of the temporal variation of backscatter time series. The inconsistency of phenology metric detection methodology should also be aware of. Our future research direction will focus on linking the variation of backscatter-extracted phenology metrics to the dynamics of ecosystem and its response to climate change. The integration of ground observation from tower sites will allow us to better interpret the remote sensing results.

Acknowledgments The resolution-enhanced SeaWinds backscatter data were obtained from the NASA Scatterometer Climate Record Pathfinder project (http://www.scp.byu.edu). This work was supported by the National Natural Science Foundation of China under grant No. 41471369 and the Major International Cooperation and Exchange Project 'Comparative study on global environmental change using remote sensing technology' under grant No. 41120114001.

References

Begue A, Vintrou E, Saad A, Hiernaux P (2014) Differences between cropland and rangeland MODIS phenology (start-of-season) in Mali. Int J Appl Earth Obs Geoinform 31:167–170

De Beurs KM, Henebry GM (2004) Land surface phenology, climatic variation, and institutional change: analyzing agricultural land cover change in Kazakhstan. Remote Sens Environ 89:497–509

Early DS, Long DG (1996) Error characteristics of the SIR resolution enhancement algorithm. In: Proceeding of IGARSS'96. IGARSS, Lincoln, pp 24–126

Early DS, Long DG (2001) Image reconstruction and enhanced resolution imaging from irregular samples. IEEE Trans Geosci Remote Sens 39:291–302

Friedl MA, Mciver DK, Hodges JCF, Zhang XY, Muchoney D, Strahler AH, Woodcock CE, Gopal S, Schneider A, Cooper A, Baccini A, Gao F, Schaaf C (2002) Global land cover mapping from MODIS: algorithms and early results. Remote Sens Environ 83:287–302

Frison PL, Mougin E (1996) Monitoring global vegetation dynamics with ERS-1 wind scatterometer data. Int J Remote Sens 17:3201–3218

Frolking S, Fahnestock M, Milliman T, Mcdonald K, Kimball J (2005) Interannual variability in North American grassland biomass/productivity detected by SeaWinds scatterometer backscatter. Geophys Res Lett 32:L21409

Frolking ST, Mcdonald MK, Kimball J, Zhao M, Fahnestock M (2006) Evaluation of the SeaWinds scatterometer for regional monitoring of vegetation phenology. J Geophys Res 111:D17302

Frolking S, Milliman T, Palace M, Wisser D, Lammers R, Fahnestock M (2011) Tropical forest backscatter anomaly evident in seawinds scatterometer morning overpass data during 2005 drought in Amazonia. Remote Sens Environ 115(3):897–907

Frolking S, Milliman T, Seto K, Friedl MA (2013) A global fingerprint of macro-scale changes in urban structure from 1999-2009. Environ Res Lett 8(2):10pp

Ganguly S, Friedl MA, Tan B, Zhang X, Verma M (2010) Land surface phenology from MODIS: characterization of the collection 5 global land cover dynamics product. Remote Sens Environ 114(8):1805–1816

Gao F, Morisette JT, Wolfe RE, Ederer G, Pedelty J, Masuoka E, Myneni R, Tan B, Nightingale J (2008) An algorithm to produce temporally and spatially continuous MODIS-LAI time series. IEEE Geosci Remote Sens Lett 5:60–64

Gessner U, Naeimi V, Klein I, Kuenzer C, Klein D, Dech S (2013) The relationship between precipitation anomalies and satellite-derived vegetation activity in Central Asia. Glob Planet Chang 110:74–87

Hardin PJ, Jackson MW (2003) Investigating SeaWinds terrestrial backscatter: equatorial savannas of south america. Photogramm Eng Remote Sens 69:1243–1254

IPCC (2007) Climate change 2007: synthesis report. Contribution of working groups I, II and III to the fourth assessment report of the Intergovernmental Panel on Climate Change. IPCC, Geneva, 104 p

Jones MO, Jones LA, Kimball JS, McDonald KC (2011) Satellite passive microwave remote sensing for monitoring global land surface phenology. Remote Sens Environ 115:1102–1114

Jones MO, Kimball JS, Jones LA, McDonald KC (2012) Satellite passive microwave detection of North America start of season. Remote Sens Environ 123:324–333

Jönsson P, Eklundh L (2002) Seasonality extraction by function fitting to time-series of satellite sensor data. IEEE Trans Geosci Remote Sens 40:1824–1831

Jönsson P, Eklundh L (2004) Timesat – a program for analyzing time-series of satellite sensor data. Comput Geosci 30:833–845

Jönsson AM, Eklundh L, Hellström M, Bärring L, Jönsson P (2010) Annual changes in MODIS vegetation indices of Swedish coniferous forests in relation to snow dynamics and tree phenology. Remote Sens Environ 114(11):2719–2730

Karl TR, Nicholls N, Ghazi A (1999) CLIVAR/GCOS/WMO workshop on indices and indicators for climate extremes: workshop summary. Clim Chang 42:3–7

Kimball JS, Mcdonald KC, Running SW, Frolking S (2004) Satellite radar remote sensing of seasonal growing seasons for boreal and subalpine evergreen forests. Remote Sens Environ 90:243–258

King MD, Greenstone R (eds) (1999) EOS reference handbook: a guide to NASA's earth science enterprise and the earth observing system. NASA document NP-1999-08-134-GSFC. NASA/Goddasd Space Flight Centre, Greenbelt, 361 pp

Kuenzer C, Zhao D, Scipal K, Sabel D, Naeimi V, Bartalis Z, Hasenauer S, Mehl H, Dech S, Wagner W (2009) El Niño southern oscillation influences represented in ERS scatterometer-derived soil moisture data. Appl Geogr 29(4):463–477

Lieth H (ed) (1974) Phenology and seasonal modeling. Springer, New York

Lu L, Guo H, Wang C, Li Q (2013) Assessment of the SeaWinds scatterometer for vegetation phenology monitoring across China. Int J Remote Sens 34(15):5551–5568

Lu L, Wang C, Guo H, Li Q (2014) Detecting winter wheat phenology with SPOT-VEGETATION data in the North China Plain. Geocarto Int 29(3):244–255. doi:10.1080/10106049.2012.760004

Macelloni G, Paloscia S, Pampaloni P, Santi E (2003) Global scale monitoring of soil and vegetation using SSM/I and ERS wind scatterometer. Int J Remote Sens 24:2409–2425

Madsen K, Nielsen HB, Tingleff O (eds) (2004) Methods for non-linear least squares problems. Technical University of Denmark, Copenhagen

Melaas EK, Richardson AD, Friedl MA, Dragoni D, Gough CM, Herbst M, Montagnani L, Moors E (2013) Using FLUXNET data to improve models of springtime vegetation activity onset in forest ecosystems. Agric For Meteorol 171–172:46–56

Min QL, Lin B (2006) Determination of spring onset and growing season leaf development using satellite measurements. Remote Sens Environ 104:96–102

Morisette JT, Richardson AD, Knapp AK, Fisher JI, Graham EA, Abatzoglou J (2009) Tracking the rhythm of the seasons in the face of global change: phenological research in the 21st century. Front Ecol Environ 7:253–260

Peterson TC (2005) Climate change indices. WMO Bull 54(2):83–86

Richardson AD, Keenan TF, Migliavacca M, Ryu Y, Sonnentag O, Toomey M (2013) Climate change, phenology, and phenological control of vegetation feedbacks to the climate system. Agric For Meteorol 169:156–173

Roberts JJ, Best BD, Dunn DC, Treml EA, Halpin PN (2010) Marine geospatial ecology tools: an integrated framework for ecological geoprocessing with ArcGIS, Python, R, MATLAB, and C++. Environ Model Softw 25:1197–1207

Shi J, Jackson T, Tao J, Du J, Bindlish R, Lu L, Chen KS (2008) Microwave vegetation indices for short vegetation covers from satellite passive microwave sensor AMSRE. Remote Sens Environ 112:4285–4300

Trenberth KE, Olson JG (1988a) Evaluation of NMC global analyses: 1979-87. NCAR Technical note TN-299+STR. National Center for Atmospheric Research, Boulder, 82 pp

Trenberth KE, Olson JG (1988b) Intercomparison of NMC and ECMWF global analyses: 1980–1986. NCAR Technical note TN-301+STR. National Center for Atmospheric Research, Boulder, 81 pp

Ulaby FT, Moore RK, Fung AK (eds) (1982) Microwave remote sensing: active and passive, vol. II: radar. Addison-Wesley, Reading

Wagner W, Lemoine G, Borgeaud M, Rott H (1999) A study of vegetation cover effects on ERS scatterometer data. IEEE Trans Geosci Remote Sens 37:938–948

Wang C, Fritschi FB, Stacey G, Yang Z (2011) Phenology-based assessment of energy crops in north american tallgrass prairie. Ann Assoc Am Geogr 101:742–751

Waring RH, Whitehead D, Jarvis PG (1979) The contribution of stored water to transpiration in Scots pine. Plant Cell Environ 2:309

White MA, De Beurs KM, Didan K, Inouye DW, Richardson AD, Jensen OP, O'keefe J, Zhang G, Nemani RR, Van Leeuwen WJD, Brown JF, De Wit A, Schaepman M, Lin X, Dettinger M, Bailey AS, Kimball J, Schwartz MD, Baldocchi DD, Lee JT, Lauenroth WK (2009) Intercomparison, interpretation, and assessment of spring phenology in North America estimated from remote sensing for 1982–2006. Glob Chang Biol 15:2335–2359

Zhang XY, Friedl MA, Schaaf CB, Strahler AH, Liu Z (2005) Monitoring the response of vegetation phenology to precipitation in Africa by coupling MODIS and TRMM instruments. J Geophys Res Atmos 110:D12103, 14 pp

Zhang XY, Friedl MA, Schaaf CB (2006) Global vegetation phenology from moderate resolution imaging spectroradiometer (MODIS): evaluation of global patterns and comparison with in situ measurements. J Geophys Res 111:G04017